Minimizing dispersion in flexible-momentum-compaction lattices

S.Y. Lee,* K.Y. Ng, and D. Trbojevic†
Fermi National Accelerator Laboratory, P.O. Box 500, Batavia, Illinois 60510
(Received 21 October 1992; revised manuscript received 22 June 1993)

Medium-energy accelerators are often confronted with problems during transition energy crossing, such as longitudinal microwave instability and nonlinear synchrotron motion. These problems can be avoided by an accelerator having a negative momentum-compaction factor. A modular method for designing a lattice with adjustable momentum-compaction factor is presented. The dispersion excursion of the basic flexible-momentum-compaction module can be minimized to less than the maximum dispersion of the focusing-defocusing (FODO) lattice containing the same FODO cells. The phase advance of the module can be adjusted to be an odd multiple of quarter betatron waves. We found that a lattice composed of such modules possesses excellent chromatic properties with excellent tunability, smaller systematic stop-band widths, and smaller sextupole distortion functions.

PACS number(s): 41.85.−p, 29.20.Lq, 29.27.−a

I. INTRODUCTION

The deviation of the revolution period ΔT for an off-momentum particle at momentum $p_0 + \Delta p$ relative to that of the synchronous (on-momentum) particle at momentum p_0 and revolution period T_0 is given by

$$\frac{\Delta T}{T_0} = \left(\alpha - \frac{1}{\gamma^2}\right)\frac{\Delta p}{p_0}\,, \tag{1.1}$$

where the $\eta = \alpha - \gamma^{-2}$ is called the phase-slip factor, γ is the Lorentz relativistic factor for the on-momentum particle, and α is the momentum-compaction factor, which measures the path length difference ΔC between the off-momentum particle and the on-momentum particle, i.e., $\frac{\Delta C}{C_0} = \alpha\frac{\Delta p}{p_0}$, where C_0 is the circumference of the reference orbit. To the lowest order in $\Delta p/p_0$, the momentum-compaction factor is related to the horizontal momentum-dispersion function $D(s)$ by

$$\alpha = \frac{1}{C_0}\oint \frac{D(s)}{\rho(s)}ds\,, \tag{1.2}$$

where ρ is the radius of curvature and s is the longitudinal path length measured along the reference orbit. During the acceleration of beam particles, the phase-slip factor changes sign as γ crosses $\gamma_t = \alpha^{-1/2}$. The particle energy at γ_t is called the *transition* energy.

There are many unfavorable effects on the particle motion around transition energy. The momentum spread of a bunch around transition can become so large that it exceeds the available momentum aperture and beam loss occurs. There is little or no Landau damping against microwave instability near transition [1]. As a result, the bunch area grows due to the space-charge force of the beam as well as due to the wake forces created by the bunch inside the vacuum chamber. Particles with different momenta may cross transition at different times leading to longitudinal phase-space distortions and beam loss.

To avoid all the above unfavorable effects, it is appealing to eliminate transition crossing. A γ_t jump mechanism was proposed by Lee and Teng [2] to ease beam dynamics problems associated with the transition crossing, where a special set of quadrupoles are pulsed so that the transition energy is lowered or raised during the transition-energy crossing. Such a scheme has become routinely operational at the CERN Proton Synchrotron and at the Fermilab Booster [3]. Alternately, the lattice having a very *small* or even *negative* momentum-compaction factor can also be designed. Vladimirski and Tarasov [4] introduced reverse bends in an accelerator lattice and succeeded in getting negative orbit-length increase with momentum, thus making a negative momentum-compaction factor. Teng [5] discovered that the same can be accomplished with a negative dispersion at dipole locations. The dispersion closed orbit can be bridged by a straight section with a phase advance of π to yield little or no contribution to positive orbit-length increment. Such a concept forms the basis of the *flexible-momentum-compaction* (FMC) lattices.

A FMC lattice requires parts of the lattice to have negative momentum dispersion functions. In the thin-lens approximation, the momentum-compaction factor in Eq. (1.2) can be written as

$$\alpha = \frac{1}{\gamma_t^2} \approx \frac{1}{C_0}\sum_i \bar{D}_i\theta_i\,, \tag{1.3}$$

where θ_i is the bending angle of the ith dipole and $\bar{D}_i$ is the average dispersion function in dipole i. The transition gamma γ_t will be an imaginary number if the momentum compaction factor α is less than zero. Thus the condition for an imaginary γ_t lattice is to have negative horizontal dispersion through most of the dipoles: $\sum_i \bar{D}_i\theta_i < 0$; i.e., $\bar{D}_i < 0$ in most of the dipoles.

An alternative method to design an FMC lattice is usually called the *harmonic approach* [6–9]. This method creates a systematic closed-orbit stop band near to the betatron tune to induce dispersion-wave oscillations resulting in a high γ_t or an imaginary γ_t. However, the resulting lattice is less tunable and the dispersion function can be large as well [6]. Thus the dynamical aperture may be reduced accordingly. The shortcomings of all these methods are (1) the π insertions lead to extra and

sometimes unwanted space in the accelerator ring and (2) large maximum and minimum local position dispersion. As an illustration, the infinite γ_t example given by Teng [5] for the Fermilab Main Ring has dispersion varying between -34.0 and 43.8 m. In fact, Teng pointed out that this is the price one has to pay for infinite transition energy.

Recently, Trbojevic and co-workers [10, 11] reintroduced a *modular approach*, similar to that of Teng's modular approach, for the FMC lattice with a controllable dispersion function. They analyzed the flow of the dispersion vector and constructed carefully matched modules of negative dispersion. These modules can be positioned one after another to create a large ring with a negative momentum-compaction factor or an imaginary γ_t. This paper makes further investigation of the method. We find that the module can be made very compact without much unwanted empty space, and at the same time, the maximum of the dispersion function can be controlled to less than that of the regular focusing-defocusing (FODO) lattice, thus overcoming both of the difficulties of Teng's original idea.

This paper is organized as follows. The method of dispersion vector is illustrated in Sec. II. In Sec. III an analytic design of the FMC module is given. In Sec. IV, realistic modules with controlled dispersion and imaginary γ_t are constructed and analyzed. In Sec. V, the incorporation of the FMC module in the Fermilab Main Injector lattice is briefly discussed together with its beam dynamics issues. A Fourier analysis of the FMC module is given in Sec. VI, which explains why our dispersion is not governed by the claim of Ref. [5]. The conclusions are given in Sec. VII.

II. REVIEW OF THE METHOD OF DISPERSION ANALYSIS

Dispersion control is the most important issue in the FMC lattice. The dispersion function D satisfies a second-order inhomogeneous differential equation of motion,

$$D'' + K_x(s)D = \frac{1}{\rho(s)} , \tag{2.1}$$

where the prime denotes the derivative with respect to the longitudinal coordinate s, $\rho(s)$ is the local radius of curvature, and

$$K_x = \frac{1}{\rho^2} - \frac{1}{B\rho}\frac{\partial B_y}{\partial x} \tag{2.2}$$

is the sum of the quadrupole and centrifugal focusings. The normalized dispersion vector with components ξ and χ is defined as

$$\xi = \sqrt{\beta_x}D' - \frac{\beta_x'}{2\sqrt{\beta_x}}D = \sqrt{2J}\cos\phi ,$$

$$\chi = \frac{1}{\sqrt{\beta_x}}D = \sqrt{2J}\sin\phi , \tag{2.3}$$

where β_x and β_x' are, respectively, the horizontal betatron amplitude function and its derivative [12], J is the dispersion action, $\sqrt{2J}$ is the amplitude of the normalized dispersion vector, and ϕ is identical to the horizontal Floquet betatron phase advance in the region where there is no dipole. In the thin-element approximation, Eq. (2.1) indicates that $\Delta D = 0$ and $\Delta D' = \theta$ in passing through a thin dipole with bending angle θ. Therefore, in the normalized ξ-χ space, the normalized dispersion vector changes by $\Delta\xi = \sqrt{\beta_x}\theta$ and $\Delta\chi = 0$. Outside the dipoles ($\rho = \infty$), the dispersion function satisfies the homogeneous equation, so that J is an invariant, with ξ and χ satisfying $\xi^2 + \chi^2 = 2J$, which is a circle, and the normalized dispersion vector advances by an angle ϕ equal to the betatron phase advance. The dispersion plots of a FODO cell and a FMC module are given in Fig. 1, whereas their thin-element approximations are shown in Fig. 2. Although they look different, the thin-element approximations are good enough in the preliminary design when dispersion control and dispersion matching are required. This type of plot has been successfully used

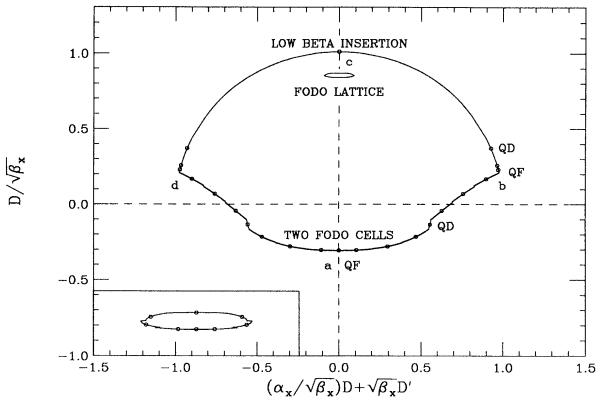

FIG. 1. Normalized dispersion ξ-χ plot for the basic module and its corresponding FODO lattice, which is magnified in the inset.

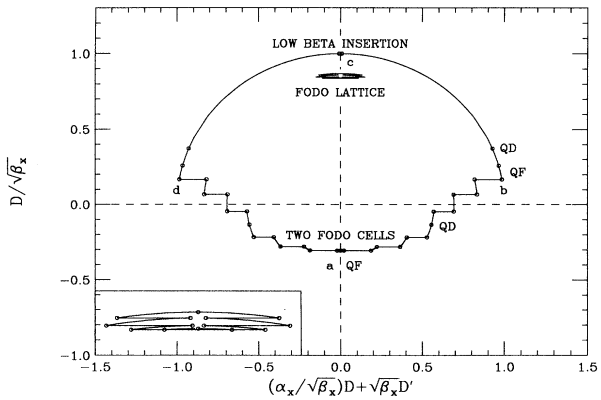

FIG. 2. Normalized dispersion ξ-χ plot for the same basic module and FODO lattice (magnified in the inset) of Fig. 1, but in the thin-element approximation. Except for the one at marker M_c where the betatron function is extremely small, all thin dipoles can be seen as horizontal lines.

in lattice design and beam-transfer line design. It has also been used to lower the dispersion excursion during a fast γ_t jump at RHIC [13] and to design a low-emittance isochronous electron ring [14].

III. THE BASIC MODULE

A basic FMC module is made of two parts: (1) the FODO cell part where the negative dispersions in the dipoles provide a negative momentum-compaction factor and (2) a matching section which matches the optical functions. Let us assume a reflective symmetry of all Courant-Snyder functions within the module with respect to the vertical χ axis in the normalized dispersion space. Although this is not a necessary condition, the reflection symmetry simplifies the analysis and optical matching considerably. The basic module containing two FODO cells can therefore be expressed as

$$M_a \left\{\tfrac{1}{2}Q_F\, B\, Q_D\, B\, \tfrac{1}{2}Q_F\right\} M_b \left\{Q_{F_1}\, O_1\, Q_{D_2}\, O_2\right\} M_c + (\text{reflective symmetry beam line}) , \tag{3.1}$$

where $M_{a,b,c}$ are marker locations, Q's are quadrupoles, O's are drift spaces, and B's stand for dipoles.

The horizontal betatron transfer matrix of the FODO cell from marker M_a to marker M_b is given by

$$M_{\text{FODO}} = \begin{pmatrix} \cos\mu & \beta_F \sin\mu & D_F(1-\cos\mu) \\ -\dfrac{1}{\beta_F}\sin\mu & \cos\mu & \dfrac{D_F}{\beta_F}\sin\mu \\ 0 & 0 & 1 \end{pmatrix} , \tag{3.2}$$

where μ is the horizontal phase advance in the FODO cell, β_F and D_F are, respectively, the betatron amplitude and dispersion functions at the center of the focusing quadrupole for the regular FODO cell, with symmetry condition $\beta'_F = 0$ and $D'_F = 0$. In the thin-lens approximation with equal focusing and defocusing strengths, the Courant-Snyder parameters are given by

$$\sin\frac{\mu}{2} = \frac{L_F}{2f} , \quad \beta_F = \frac{2L_F\left(1+\sin\dfrac{\mu}{2}\right)}{\sin\mu} ,$$

$$D_F = \frac{L_F\theta\left(2+\sin\dfrac{\mu}{2}\right)}{2\sin^2\dfrac{\mu}{2}} , \tag{3.3}$$

where L_F is the length of the half FODO cell, f is the focal length of quadrupoles in the FODO cell, and θ is the bending angle of the dipole B. However, it is worth pointing out that the applicability of Eq. (3.2) is not limited to thin-lens approximation.

To build a module with a negative momentum-compaction factor, most of the dipoles should be within the third and fourth quadrants of the (ξ,χ) normalized dispersion space. The dispersion function at the beginning of the FODO cell is prescribed with a negative value D_a with $D'_a = 0$. As we shall see, the choice of D_a is essential in determining dispersion excursion and γ_t value of the module. Using the transfer matrix in Eq. (3.2), the dispersion function at marker M_b is found to be

$$D_b = D_F - (D_F - D_a)\cos\mu , \quad D'_b = \frac{D_F - D_a}{\beta_b}\sin\mu , \tag{3.4}$$

where β_b is the betatron amplitude function at marker M_b with $\beta_b = \beta_F$. In the matching section (assuming that there is no dipole contribution to dispersion), the dispersion action is invariant given by

$$J_c = J_b = \frac{1}{2}\left[\frac{D_b^2}{\beta_b} + \beta_b D_b'^2\right] = J_F[1-2(1-\zeta)\cos\mu+(1-\zeta)^2] . \tag{3.5}$$

with $\zeta = D_a/D_F$ as the ratio of the desired dispersion at marker M_a and

$$2J_F = L_F\theta^2 \frac{\cos\dfrac{\mu}{2}\left(1+\dfrac{1}{2}\sin\dfrac{\mu}{2}\right)^2}{\sin^3\dfrac{\mu}{2}\left(1+\sin\dfrac{\mu}{2}\right)} \tag{3.6}$$

as the action for the regular FODO cell at the focusing quadrupole location. Figure 3 shows $\sqrt{J_b/J_F}$ as a function of ζ for various phase advances per cell. Note that the ratio of the dispersion norms increases when the initial dispersion D_a at marker M_a is chosen to be more negative. It is preferable to have a smaller dispersion action in the matching section in order to minimize the dispersion function of the module. One may like to con-

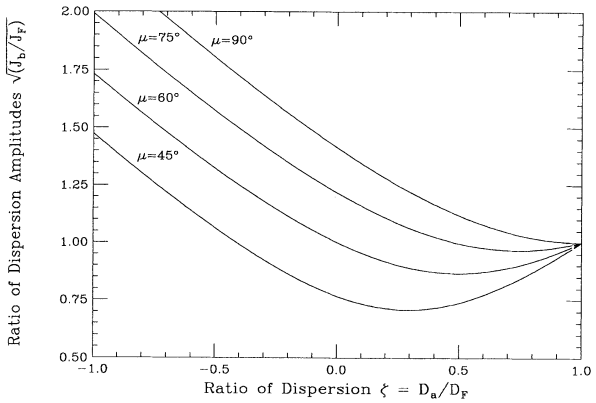

FIG. 3. Ratio of dispersion amplitudes $\sqrt{J_b/J_F}$ as a function of $\zeta = D_a/D_F$ for various phase advances μ in the FODO cell.

clude from Fig. 3 that a smaller phase advance in the FODO cell is preferred. This is true if we are comparing the dispersion of the basic module only with the regular FODO lattice that contains the same FODO cells. However, it is worth pointing out that the dispersion amplitude $\sqrt{2J_F}$ in Eq. (3.6) is inversely proportional to $(\sin\frac{\mu}{2})^{3/2}$. To obtain a smaller $\sqrt{2J_c}$, we should properly choose the phase advance for the FODO cell. A compromised choice for the phase advance of the FODO cell is between 60° and 75°. In order to further reduce the dispersion at marker M_c, and to shorten the matching section, a low-horizontal-betatron-amplitude (low-β) insertion is desired.

The dispersion functions and other Courant-Snyder parameters are then matched at the symmetry point at marker M_c with a doublet (or triplet). The betatron transfer matrix is given by

$$M_{b\to c}=\begin{pmatrix} \sqrt{\frac{\beta_c}{\beta_b}}\cos\psi & \sqrt{\beta_b\beta_c}\sin\psi & 0 \\ -\frac{1}{\sqrt{\beta_b\beta_c}}\sin\psi & \sqrt{\frac{\beta_b}{\beta_c}}\cos\psi & 0 \\ 0 & 0 & 1 \end{pmatrix}, \tag{3.7}$$

where we have also assumed a symmetry condition at marker M_c for the Courant-Snyder parameters, i.e., $\beta_b'=0$ and $\beta_c'=0$. Here, β_b and β_c are the betatron amplitudes at, respectively, markers M_b and M_c, while ψ is the betatron phase advance between markers M_b and M_c.

The required dispersion matching condition at marker M_c is $D_c'=0$. Using Eq. (3.4), we obtain then

$$\tan\psi=\frac{(1-\zeta)\sin\mu}{1-(1-\zeta)\cos\mu}\,. \tag{3.8}$$

This means that the phase advance of the matching section is not a free parameter, but is determined completely by the initial dispersion value D_a at marker M_a and the phase advance of the FODO cell. This condition is independent of whether we use a FODO-type insertion or a low-β insertion with doublets or triplets for the matching section. Such a matching section differs from that in Teng's module, which specifies an exact π insertion [5]. Figure 4 shows the required phase advance in the matching section as a function of phase advance μ of the FODO cell for various values of $\zeta=D_a/D_F$. The total phase advance of the whole basic module is then given by $2(\mu+\psi)$, which is a function of only the desired dispersion function at marker M_a and the phase advance μ in the FODO cell. Figure 5 shows the total phase advance of the whole module as a function of the phase advance of the FODO cell for $\zeta=-0.3$ to -0.6.

Quadrupoles Q_{F_1} and Q_{D_2} in the matching section are then adjusted to achieve the required phase advance ψ given by Eq. (3.8) and to produce a low betatron amplitude function at marker M_c. Care should also be taken in the arrangement and choices of quadrupoles Q_{F_1} and Q_{D_2} in order to achieve reasonably small vertical Courant-Snyder parameters. Then, the matching becomes relatively simple. From the beam dynamics point of view, a basic module with a phase advance of $\frac{3}{2}\pi$ is

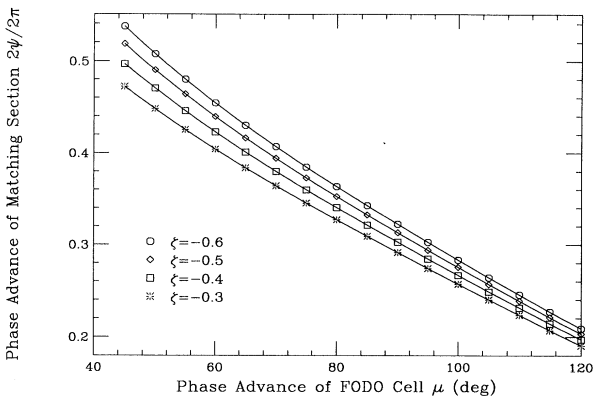

FIG. 4. Phase advance in the matching section as a function of phase advance μ in the FODO cell for various $\zeta=D_a/D_F$.

preferable due to the cancellation in the systematic half-integer stop band and the sextupole distortion functions. To achieve a $\frac{3}{2}\pi$ phase advance, $\zeta\approx-0.3$ to -0.4 and a phase advance per FODO cell of $\mu=60°$ to 75° can be used.

The dispersion values at the midpoints of dipoles in the FODO cell are given by

$$D_{B_1}=D_a(1-\tfrac{1}{2}\sin\tfrac{1}{2}\mu),$$

$$D_{B_2}=D_a(1-\tfrac{1}{2}\sin\tfrac{1}{2}\mu)+(D_F-D_a)\sin^2\tfrac{1}{2}\mu. \tag{3.9}$$

In the thin-element approximation, the momentum compaction becomes

$$\alpha=\frac{(D_{B_1}+D_{B_2})}{L_m}\theta\,, \tag{3.10}$$

where θ is the bending angle of each dipole and L_m is the length of the half-module. In comparison with the momentum-compaction factor of a lattice composed entirely of conventional FODO cells, we obtain

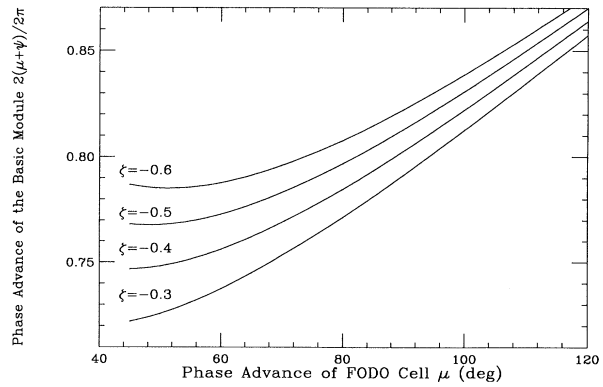

FIG. 5. Total phase advance of the whole module as a function of phase advance μ in the FODO cell for various $\zeta=D_a/D_F$.

$$\frac{\alpha}{\alpha_{\rm FODO}} = \frac{2L_F}{L_m}\left[\zeta + (1-\zeta)\frac{\sin^2\frac{1}{2}\mu}{2-\sin\frac{1}{2}\mu}\right] . \qquad (3.11)$$

Note that the momentum-compaction factor of the module is determined entirely by the choice of D_a, the phase advance of the FODO cell, and the ratio of the lengths of the FODO cell and the module. When the length of the module is a constant, the momentum-compaction factor depends linearly on the initial value of the dispersion function D_a. Although the thin-lens approximation has been used for the quadrupoles and dipoles, it is easy to see that this linear relationship is exact even for thick elements. If the horizontal phase advance μ_x of the FODO cell is different from its vertical phase advance μ_y, Eqs. (3.9) and (3.11) still hold when the replacements

$$\sin^2\tfrac{1}{2}\mu \to \sin^2\tfrac{1}{2}\mu_x ,$$
$$\tfrac{1}{2}\sin\tfrac{1}{2}\mu \to \tfrac{1}{8}(s_- + \sqrt{s_-^2 + 8s_+}) \qquad (3.12)$$

are made, where $s_\pm = \sin^2\frac{1}{2}\mu_x \pm \sin^2\frac{1}{2}\mu_y$.

The above analysis can be applied also to a DOFO cell discussed in our previous study [11]. In the case with DOFO cells, the variables with the subscript F in Eqs. (3.1) to (3.4) should be replaced with the values at the defocusing quadrupole. In fact, J_D is slightly larger than J_F. A slightly smaller $|\zeta|$ has to be used in order to minimize the magnitude of the dispersion function in the module, because the dispersion value at the defocusing quadrupole location is smaller than that at the focusing quadrupole location. From Fig. 5, we observe therefore that a larger phase advance should be used in the low-β matching section, where a triplet should be used. It becomes more difficult, however, to achieve the condition of $\frac{3}{2}\pi$ phase advance in the basic module.

For some economical reasons, one may try to use DOFODO in place of the FODO cell in Eq. (3.1), i.e., three FODO cells instead of two are placed inside a basic module. The betatron transfer matrix in the DOFODO cell becomes

$$M_{a\to b} = \begin{pmatrix} \sqrt{\frac{\beta_F}{\beta_D}}\cos\frac{3}{2}\mu & \sqrt{\frac{\beta_F}{\beta_D}}\sin\frac{3}{2}\mu & D_F - D_D\sqrt{\frac{\beta_F}{\beta_D}}\cos\frac{3}{2}\mu \\ -\frac{1}{\sqrt{\beta_F\beta_D}}\sin\frac{3}{2}\mu & \sqrt{\frac{\beta_D}{\beta_F}}\cos\frac{3}{2}\mu & \frac{D_D}{\sqrt{\beta_F\beta_D}}\sin\frac{3}{2}\mu \\ 0 & 0 & 1 \end{pmatrix} , \qquad (3.13)$$

where μ is the phase advance of a FODO cell, β_F, β_D, D_F, and D_D are, respectively, betatron amplitudes and dispersion values at the focusing and defocusing quadrupoles of the FODO cell. A similar analysis with a different number of FODO cells can be repeated easily. In general, the result will be a larger total dispersion value with less favorable phase advance for the module.

IV. CONSTRUCTION AND ANALYSIS OF REALISTIC BASIC MODULE

Since the dispersion function of the basic module is a free parameter, the momentum-compaction factor of Eq. (1.3) can be varied. As an example, we consider a basic module made of two FODO cells, each of length 27.16 m, and a reflective symmetric insertion consisting of two quadrupole doublets. There is one dipole of length 9.45 m and bending angle 38.924 mrad in each of the half FODO cells. A dipole of length 2.953 m with bending angle 12.163 mrad is located at the center of the symmetric insertion in order to increase the packing factor of the lattice. The length of the module is chosen to be 72 m except when the module has large positive momentum compaction. To achieve negative momentum compaction, the horizontal and vertical phase advances of this module will vary from 0.835 to 0.760 for ν_x and from 0.937 to 0.814 for ν_y.

The betatron phase advances of the FODO cell are first fixed at $\mu_x/2\pi$ =0.181 and $\mu_y/2\pi$ =0.295, respectively. The betatron functions at the center of the F quadrupole are then $\beta_x = 52.825$ m and $\beta_y \cong 44.5$ m. For a regular FODO cell lattice, the dispersions at the F and D quadrupoles are $D_F = 2.529$ m and $D_D = 1.289$ m, respectively. Table I shows the dependence of the momentum-compaction factor as a function of the initial dispersion $D_{\rm min}$ at marker M_a. Table I shows that the momentum-compaction factor α changes sign at $D_{\rm min} \approx -0.885$ m, where the γ_t value becomes very large, while the betatron functions do not change appreciably. Figure 6 shows the normalized dispersion phase space plot in ξ-χ plane for these lattices with varying $D_{\rm min}$.

When the starting value of the $\chi_{\rm min} \approx -0.125$, as is presented in Fig. 6, the momentum-compaction factor is very close to zero or γ_t becomes a large imaginary value (one example is presented where $\gamma_t = i104.38$) or a large real value (one case is presented where $\gamma_t = 223.65$). Any small changes of the tunes for these modules will produce a large change in γ_t. They are useful in the design of *isochronous* lattices. The momentum-compaction factor is plotted against the initial dispersion $D_{\rm min}$ in Fig. 7. We observe a linear relationship except for the three points at the far right which are of considerably smaller modular lengths needed in the matching.

The momentum-compaction factor becomes zero (isochronism) at $\zeta = -0.261$ ($D_{\rm min} = -0.660$ m) obtained from Eq. (3.11). However, this occurs actually at $\zeta = -0.35$ ($D_{\rm min} = -0.885$ m) as shown in Fig. 7. The

TABLE I. Variation of γ_t as a function of $D_{\min}$ showing modules with FODO cells of fixed tunes: $\nu_x = 0.181$, $\nu_y = 0.295$.

γ_t	ν_x	ν_y	$D_{\max}$ (m)	$D_{\min}$ (m)
$i23.275$	0.83579	0.93727	0.81343	−2.50000
$i26.935$	0.81710	0.85538	0.77439	−2.00000
$i35.039$	0.79452	0.76733	0.77516	−1.50000
$i80.440$	0.76767	0.80456	0.98849	−1.00000
$i461.607$	0.76033	0.81404	1.03838	−0.88000
$i671.104$	0.76021	0.81421	1.03923	−0.87800
$i789.966$	0.76018	0.81425	1.03944	−0.87750
$i1007.845$	0.76014	0.81429	1.03965	−0.87700
816.158	0.76002	0.87500	1.04071	−0.87500
502.835	0.75989	0.87300	1.04131	−0.87300
268.897	0.75939	0.81531	1.04472	−0.86500
120.311	0.75652	0.81882	1.06317	−0.82000
80.518	0.75196	0.82604	1.09472	−0.75000
47.123	0.73448	0.84777	1.19941	−0.50000
36.859	0.71503	0.87015	1.29385	−0.25000
25.266	0.64343	0.92643	1.62542	0.42900
21.574	0.58485	0.93472	1.83655	0.66500
18.841	0.52070	0.90784	2.04859	0.87400
15.885	0.42758	0.89983	2.67670	1.17600

discrepancy is due to the positive contribution of the extra dipole in the low-β matching section of the module which has not been included in the analytic model. Nevertheless, the analytic formula provides a valuable guide in the design of the modules.

The rule for the choice of the phase advances within a FODO cell is different in the *modular* imaginary γ_t lattice design. For the conventional FODO cell design, the phase advance of a FODO cell is usually chosen to be 90° or 60°. The 90° phase advance is preferred to obtain a smaller dispersion function. On the other hand, the dispersion function for the FMC lattice reaches minimum at about 60° phase advance. The magnitude of dispersion function of FMC lattice is about half of the corresponding regular FODO cell lattice. To illustrate this point, three modules, made of the same magnetic elements but with different horizontal betatron phases within the FODO cells, were constructed to produce the same value of imaginary $\gamma_t \sim i45$. The vertical tune within the FODO cells was kept the same at $\nu_y = 0.255$ in these three examples. Figure 8 shows the dependence of the minimum dispersion value on the horizontal betatron phase advance of the FODO cell. They are, respectively 90°, 68.4° and 52.2°, for which β_F is roughly the same. It is clear that the module with 52.2° FODO cells provides the smallest negative dispersion at marker M_a.

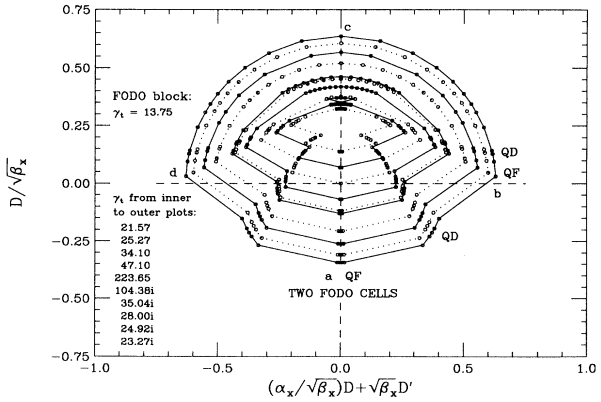

FIG. 6. The normalized dispersion phase space (ξ, χ) for various lattices with different γ_t values given in Table I with the same FODO cell are compared.

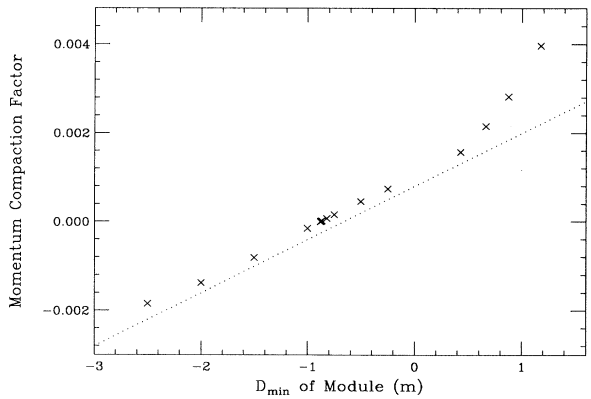

FIG. 7. Plot of momentum-compaction factor as a function of minimum dispersion for the modules discussed in Table I and Fig. 6. The dotted line is the linear relationship predicted analytically by Eq. (3.10) with the dipole in the low-β matching section omitted.

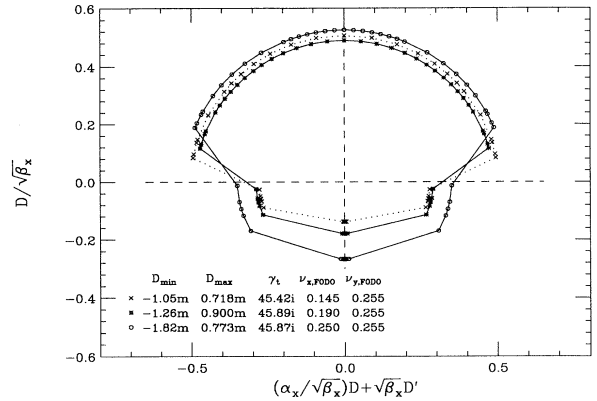

FIG. 8. Normalized dispersion ξ-χ plots for a basic imaginary γ_t module with different phase advances for the FODO cell section.

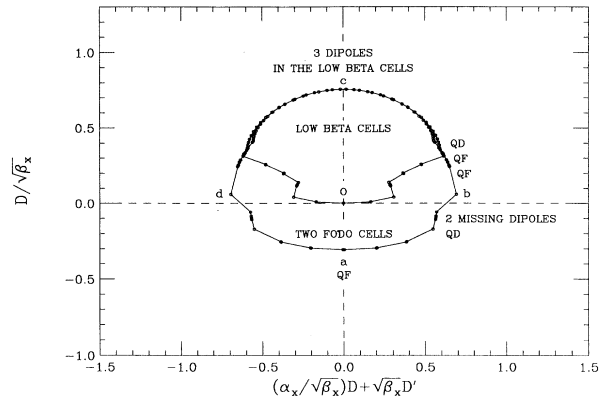

FIG. 10. Normalized dispersion ξ-χ plot for the zero-dispersion long straight.

V. A PRACTICAL EXAMPLE

There has been a desire to avoid transition crossing in the Fermilab Main Injector by making γ_t imaginary. We construct a FMC basic module with twelve 6.096-m 20.94-mrad dipoles within the two 58° FODO cells (three per half cell) and one dipole in the low-β insertion. The focusing and defocusing quadrupoles, of length 0.988 m, have gradients 220.6 and −216.8 kG/m, respectively. The first F quadrupole in each doublet of the insertion shares the same function of the last focusing quadrupole of the FODO cell. This not only eliminates one FODO quadrupole, but also shortens the length of the module, making it more compact. The total length of the module is 112.1 m with $\gamma_t = i28.65$. The minimum and maximum of the dispersion function are −2.700 m and +2.064 m. In spite of the 2.084 m low β at marker M_c, the largest horizontal betatron function at the doublet is still slightly less than the 77.39-m value of the FODO cell at marker M_a. The largest vertical betatron function is 79.11 m. The normalized dispersion vector for this module in the ξ-χ space is shown in Fig. 1, and the lattice with its Courant-Snyder properties is shown in Fig. 9.

Long zero-dispersion straight sections are important in the high-energy accelerator for locating devices such as accelerating cavities, spin rotators, etc. For the FMC lattice, the zero-dispersion straight module can be achieved with the missing-dipole scheme. This module resembles a set of two basic FMC modules with some dipoles omitted. The flow of the dispersion vector in the ξ-χ space is shown in Fig. 10 and the lattice in Fig. 11. This module starts from the same point a, and follows path from b to c, and curves back to the origin O, where both D and D' are equal to zero. The entire straight section with zero dispersion is represented by a point at the origin. To curve the dispersion vector from marker M_c back to the origin O, the last dipole in the zero-dispersion suppression cell should be placed close to the ξ axis at the negative side so that its end would be exactly at the origin O. Figure 10 also shows that the two missing dipoles at the end of the FODO cell are necessary to provide for smaller radius of the closure circle. This module has a positive momentum-compaction contribution of $\alpha = 0.000\,591$ and a length of 329.22 m, of which the zero-dispersion part spans 80 m.

Beam dynamics issues are also important to lattice performance. The beam dynamics properties of a whole lattice built from putting together a number of basic blocks, two zero-dispersion straight blocks, and a few extraction-injection blocks have been studied seriously [15]. We find

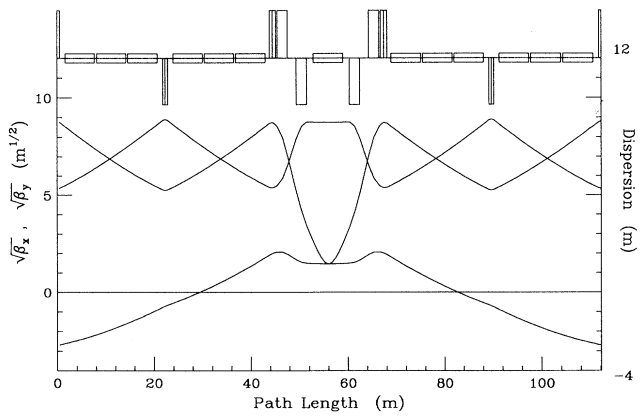

FIG. 9. Betatron and dispersion functions for the basic module of the imaginary γ_t lattice.

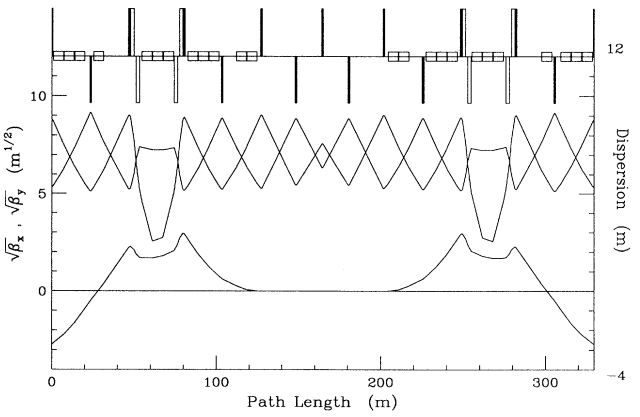

FIG. 11. Betatron and dispersion functions for the dispersion-free module of the imaginary γ_t lattice.

that this lattice is extremely tunable and is insensitive to misalignment errors. Its chromatic properties are at least comparable to that of the regular FODO lattice. Since each basic module and extraction-injection module has phase advance close to 0.75, the distortion functions of the sextupoles necessary for chromaticity corrections cancel for every block of four modules. This applies to the systematic half-integer stop band also. As a result, the lattice provides dynamical aperture as large as that of the regular FODO lattice. A detailed analysis is given in Ref. [15].

VI. FOURIER ANALYSIS

An alternate way to understand the dispersion excursion of the FMC module is the method of Fourier analysis [12]. For a reflectively symmetric module starting from marker M_a, the Fourier coefficients are defined by

$$a_k = \frac{1}{\pi\nu}\int_0^{\pi\nu} d\psi \frac{\beta^{3/2}}{\rho(s)}\cos k\frac{\psi}{\nu} \tag{6.1}$$

for $k = 0, 1, 2, \ldots$. Here $2\pi\nu$ is the total phase advance of the module. The local dispersion $D(s)$ and momentum compaction factor α of the module are then given by

$$D(s) = \beta^{1/2}\left[a_0 + \sum_{k=1,2,\ldots}\frac{2a_k\cos k\frac{\psi}{\nu}}{1-(k/\nu)^2}\right], \tag{6.2}$$

$$\alpha = \frac{\pi\nu}{L_m}\left[a_0^2 + \sum_{k=1,2,\ldots}\frac{2a_k^2}{1-(k/\nu)^2}\right], \tag{6.3}$$

where $2L_m$ is the length of the module.

The first few Fourier coefficients are usually of the same order of magnitude, although a_0 is a little bit larger. For a lattice composed of FODO cells only, the coefficient a_0 alone determines the local dispersion and momentum-compaction factor because $\nu \lesssim \frac{1}{4}$ for a FODO cell and therefore the contributions of the Fourier coefficients a_k are small for $k \neq 0$. For the basic module that we discussed in the Sec. V, $\nu \approx 0.75$ with $\mu \approx 60°$, thus the Fourier harmonics $k = 0$ and 1 are important. The contributions of the first few harmonics are listed in Table II.

The momentum-compaction factor is given by

$$\alpha \approx \frac{\pi\nu}{L_m}\left[a_0^2 - \frac{2a_1^2\nu^2}{1-\nu^2}\right]. \tag{6.4}$$

The a_1^2 term is larger than the a_0^2 term resulting in a negative momentum-compaction factor. The dispersions at marker M_a and M_c are, respectively,

$$D_a \approx \beta_F^{1/2}\left[a_0 - \frac{2a_1\nu^2}{1-\nu^2}\right], \quad D_c \approx \beta_c^{1/2}\left[a_0 + \frac{2a_1\nu^2}{1-\nu^2}\right]. \tag{6.5}$$

Since a_0 and a_1 are both positive and less than unity so that D_a arrives from the difference of two terms, it is possible to make $|D_a|$ less than the D_F for a regular FODO lattice. On the other hand, D_c, being the sum of two terms, can be made small also due to the small value of the betatron function β_c. Thus the maximum positive and negative dispersions of the FMC module discussed in Sec. III are less than $\frac{1}{2}$ of that of the corresponding FODO lattice. The design method of present FMC module circumvents difficulties of high dispersion function in earlier attempts of the FMC lattice design [5]. The ability to achieve a small dispersion is due mainly in part to the adjustable phase advance of the matching section with only two FODO cells in the basic module.

On the other hand, the module discussed in Ref. [5] consists of fifteen 59° FODO cells and an exact π matching insertion. The tune of module is $\nu = 2.96$, implying that the normalized dispersion vector winds around the origin of the ξ-χ space three times. The contributions of the first few Fourier coefficients are listed in Table II. Although the π insertion is not symmetric, the imaginary parts of a_k are very small and only the real parts of a_k are listed. Since ν is very close to 3, the contribution of the $k = 3$ harmonic to the momentum-compaction factor is very strong. In fact, it cancels the contributions of $k = 0$, 1, and 2 so as to make the module nearly isochronous. The local dispersion depends on the first power of a_k only, unlike the momentum-compaction factor which depends on the second power. Since all $|a_k| < 1$, the dispersions at markers M_a and M_c is dominated by the $k = 3$ term alone. This term is large because ν is very close to 3, and so are the dispersion functions. A

TABLE II. Contributions of various harmonics to momentum compaction factor and dispersions at markers M_a and M_c.

k	a_k ($m^{1/2}$)	Contribution to α	Contribution to $D_a/\beta_a^{1/2}$ ($m^{1/2}$)	Contribution to $D_c/\beta_c^{1/2}$ ($m^{1/2}$)
		Our basic module		
0	0.3734	0.0059	0.3734	0.3734
1	0.2519	−0.0070	−0.6575	0.6575
2	0.0505	−0.0000	−0.0167	−0.0167
		Teng's module		
0	0.4435	0.0035	0.4435	0.4435
1	0.0858	0.0003	0.1937	−0.1937
2	−0.0736	0.0004	−0.2707	−0.2707
3	0.0556	−0.0041	−4.1041	4.1041
4	−0.0350	−0.0005	0.0847	0.0847

similar conclusion can be reached through an FMC module composed of nine or three 59° FODO cells with a π matching section. This argument leads to the discouraging remarks that large local dispersions are deemed unavoidable in FMC lattices [5]. In fact, it is not difficult to understand that this discouraging conclusion is a direct result of the exact π phase advance of the matching section and the large number of FODO cells in the module, although it was also mentioned in Ref. [5] that an exact π insertion is unnecessary.

On the other hand, when the phase advance of the matching insertion of a basic FMC module is relaxed, the tune of the module can be adjusted to $\nu \approx 0.75$, which leads to controllable momentum-compaction value and dispersion functions discussed earlier. In fact not all parameters ζ, $\sqrt{2J}_c/\sqrt{2J}_a$, μ, ψ, and α for a basic FMC module, besides the FODO cell length and the modular length, are independent, as was discussed in Sec. III. If we restrict the phase advance of the matching section, the dispersion can no longer be minimized.

VII. CONCLUSION

In conclusion, we have reviewed methods of designing an accelerator or storage ring lattice with flexible momentum-compaction factor. Analytic formulas as well as numerical examples have been used to demonstrate the basic design principle of a lattice with a negative momentum compaction and small dispersion function. A basic module of the FMC lattice is made of two FODO cells matched by a reflective symmetric doublet-matching low-β insertion. Analytic analysis and numerical examples indicate that the dispersion and betatron amplitude matching can be achieved easily.

We proved analytically that the phase advance of the module is determined by two parameters, the phase advance per FODO cell in the module and the initial dispersion function at the focusing quadrupole. The magnitude of the momentum compaction factor is determined in turn by the initial dispersion value. With a proper choice of this initial value, the amplitude of the dispersion function is demonstrated to be less than that of the corresponding lattice composed of FODO cells alone. The phase advance in each module can also be adjusted to be an odd multiple of $\frac{\pi}{2}$ so as to minimize the half-integer and third-order stop-band widths, resulting in a lattice with excellent chromatic properties. With such phase advance, excellent distortion-function cancellation due to chromatic sextupoles is possible without resorting to extra families of sextupoles. Therefore, the dynamical aperture achieved in the present imaginary γ_t lattice is at least as large as that of the regular FODO cell lattice.

A major advantage of the imaginary γ_t lattice is that transition crossing is avoided. Because the momentum-compaction factor is negative, the longitudinal motion of beam particles is always below transition where the space-charge impedance does not cause microwave instability. The longitudinal phase-space blowup and possible beam loss due to nonlinear synchrotron motion around the transition energy region can be avoided. Applying the imaginary γ_t design principle, a lattice with zero momentum-compaction factor, or the *isochronous* storage ring, can be designed with excellent beam dynamics properties by a proper choice of the dispersion function.

* Permanent address: Department of Physics, Indiana University, Bloomington, IN 47405.
† Present address: Brookhaven National Laboratory, Upton, NY 11973.

[1] S.Y. Lee and J.M. Wang, IEEE Trans. Nucl. Sci. **NS-32**, 2323 (1985).
[2] W.W. Lee and L.C. Teng, in *Proceedings of the Eighth International Conference on High Energy Accelerators, Geneva, 1971*, edited by M. Blewett (European Organization for Nuclear Research, Geneva, 1971), pp. 327–330.
[3] W. Hardt and D. Möhl, CERN Report No. CERN ISR-300/GS/69-16 (unpublished); W. Hardt, in *Proceedings of the Ninth International Conference on High Energy Accelerators, Stanford, 1974*, edited by R. Nelson (International Union of Pure and Applied Physics, Sweden, National Science Foundation, U.S. Atomic Energy Commission, Washington, DC, 1974), pp. 434–438; T. Riesselada, CERN Report No. CERN PS/90-51, 1990 (unpublished).
[4] V.V. Vladimirski and E.K. Tarasov, *Theoretical Problems of the Ring Accelerators* (USSR Academy of Sciences, Moscow, 1955).
[5] L.C. Teng, Part. Accel. **4**, 81 (1972).
[6] R. Gupta and J.I.M. Botman, IEEE Trans. Nucl. Sci. **NS-32**, 2308 (1985).
[7] T. Collins, Fermilab Technical Memo, 1988 (unpublished).
[8] G. Guignard, in *Proceedings of the 1989 IEEE Particle Accelerator Conference, Chicago 1989*, edited by F. Bennett and J. Kopta (IEEE, New York, 1989), pp. 915–917.
[9] E.D. Courant, A.A. Garren, and U. Wienands, in *Proceedings of the 1991 IEEE Particle Accelerator Conference, San Francisco, 1991,* edited by L. Lizama (IEEE, New York, 1991), pp. 2829–2831.
[10] D. Trbojevic, D. Finley, R. Gerig, and S. Holmes, in *Proceedings of Second European Particle Accelerator Conference, Nice, 1990*, edited by P. Marin and P. Mandrillon (Editions Frontières, Gif-sur-Yvette, France, 1990), pp. 1536–1538.
[11] K.Y. Ng, D. Trbojevic, and S.Y. Lee, in *Proceedings of the 1991 IEEE Particle Accelerator Conference* (Ref. [9]), pp. 159–161.
[12] E.D. Courant and H.S. Snyder, Ann. Phys. (N.Y.) **3**, 1 (1958).
[13] D. Trbojevic, S. Peggs, and S. Tepikian, in *Proceedings of 1993 IEEE Particle Accelerator Conference, Washington, DC, 1993*, edited by S. T. Corneliussen (IEEE, New York, in press).
[14] S.Y. Lee, K.Y. Ng, and D. Trbojevic, in *Proceedings of the 1993 IEEE Particle Accelerator Conference, Washington, DC, 1993*, (Ref. [13]).
[15] S.Y. Lee, K.Y. Ng, and D. Trbojevic, Fermilab Internal Report No. FN-595, 1992 (unpublished).